Menzyanova et al., J Biotechnol Biomater 2018, 8:3
DOI: 10.4172/2155-952X.1000284

Journal of Biotechnology & Biomaterials

Research Article Open Access

Morphological Aspects of Monocyte/Macrophage Polarization on Biopolymer Scaffolds in Atherosclerosis Patients

Natalia G. Menzyanova[1]*, Svetlana V. Pyatina[1], Elena D. Nikolaeva[1], Alexander V. Shabanov[2], Ivan V. Nemtsev[3], Dmitry P. Stolyarov[4], Dmitry B. Dryganov[4], Eugene V. Sakhnov[4], Daria A. Vinokurova[1] and Ekaterina I. Shishatskaya[1]

[1]*Siberian Federal University, Svobodny, Krasnoyarsk, Russia*
[2]*L.V. Kirensky Institute of Physics, Siberian Branch of the Russian Academy of Sciences, Krasnoyarsk, Russia*
[3]*Federal Research Centre Krasnoyarsk Scientific Centre of the Siberian Branch of the Russian Academy of Sciences, Krasnoyarsk, Russia*
[4]*Federal Centres for Cardiovascular Surgery, Krasnoyarsk, Russia*

Abstract

The morphotypes of human macrophages (MPh) were studied in the culture on nano-structured substrates, made from polyhydroxyalcanoates (PHAs) of various monomer compositions, prepared by casting polymer solutions on a defatted glass and followed by the solvent evaporation. Its surface relief, being further in direct contact with human cells *in vitro* was analyzed by AFM and SEM scanning. It was shown, that the features of micro/nano relief depend on the monomeric composition of polymer substrates. Monocytes (MNs) of patients with atherosclerosis and cardiac ischemia undergoing stenting and conventional anti-atherosclerotic therapy were harvested prior to and after stenting. After isolation MNs were cultured and transformed into MPh in direct contact with biopolymer culture substrates with different monomer composition and Nano-reliefs in comparison with culture plastic. Sub-populations of cells with characteristic morphology in each phenotypic class were described and their ratios for five samples of polymers were counted as an intermediate result in the development of "smart" material for blood vessel recovery.

The results obtained allow us to assume that the processes of MPh differentiation and polarization *in vitro* depend not only on the features of the micro/nano relief of biopolymer substrates but also on the initial state of MNs *in vivo* and the general response of patients

Keywords: Monocytes; Macrophages; Cell morphology; Polyhydroxyalkanoates; PHA; Copolymers; Atherosclerosis; Intravascular stenting

Introduction

The development of atherosclerosis is associated with impaired lipid metabolism. In blood vessels, these disorders involve increasing level of lipids, associated with the certain classes of lipoprotein (LP) activation of free radical oxidative modifications of lipids in LP and induction of the synthesis of specific antibodies to modified LP, which leads to the appearance of circulating immune complexes. These disorders are the result of long-term epigenetic rearrangements, leading to changes in the methylation level of the genes, involved in the regulatory signaling of lipid metabolism and genes encoding key enzymes of lipid metabolism [1-6].

Increased lipid level in plasma is considered to be an epigenetic factor, triggering the epigenetic rearrangements of circulating blood cells and endothelial cells of blood vessels. These epigenetic changes lead to the formation of atherosclerotic plaques, local formations in the wall of the vessel [7-10].

At the histological level an atherosclerotic plaque consists of a) monocytes-macrophages and lipid-loaded foam cells, originating from the monocytes-macrophages; b) actively proliferating smooth muscle cells; c) lymphocytes; d) developed an extracellular matrix with lipid inclusions, and e) a vascular network, developed to a different degree [11-13].

Atherosclerotic plaque is a labile system, which dynamics determines the individual clinical prognosis. Modeling molecular and cellular events in atherosclerotic plaque using *in vitro* and *in vivo* systems has made a significant contribution to our understanding of principles of atherosclerotic plaque biogenesis and the possibilities of its pharmacological regulation. However, the effectiveness of pharmacological control over the dynamics of atherosclerotic plaques in patients remains relatively low [14]. This is due to the fact, that the therapy is aimed at correcting remote of metabolic consequences of epigenetic rearrangements, which determines the pathogenesis of atherosclerosis.

An elegant engineering solution, bypassing the problem of the epigenetic nature of the disease, was found: a stent, i.e. a rigid framework, is installed in the zone of an atherosclerotic plaque and mechanically widens the lumen of the narrowed vessel. Stent materials can include drugs, inhibiting proliferative activity, thrombus formation, and inflammation. Unfortunately, the mechanical solution of the biological problem did not justify the hopes of clinical medicine, because implants often led to restenosis – the accelerated re-development of an unstable atherosclerotic plaque in the implantation zone. The frequency of restenosis when using drug-eluting stents is from 5 to 10% [15-17].

The inconsistency of the engineering approach confirmed the epigenetic nature of atherosclerosis and stimulated the development of materials, whose biological activity is determined not only by chemical groups, exposed on the surface but also by the micro- and nano-relief features of the stent material. These materials should regulate the functional activity of monocytes-macrophages with the "atherosclerotic" epigenome and prevent the re-development of molecular and cellular events, leading to restenosis.

***Corresponding author:** Natalia G. Menzyanova, Siberian Federal University, Svobodny, Krasnoyarsk, Russia, E-mail: mennage@mail.ru

Received July 19, 2018; **Accepted** September 18, 2018; **Published** September 25, 2018

Citation: Menzyanova NG, Pyatina SV, Nikolaeva ED, Shabanov AV, Nemtsev IV, et al. (2018) Morphological Aspects of Monocyte/Macrophage Polarization on Biopolymer Scaffolds in Atherosclerosis Patients. J Biotechnol Biomater 8: 284. doi: 10.4172/2155-952X.1000284

Screening the biological activity of such materials in the process requires adequate *in vitro* models. The mandatory conditions for the adequacy of such models are as follows:

- the use of monocyte-macrophage cultures as main cell components in the biogenesis of atherosclerotic plaque;

- the isolation of monocyte-macrophage from the blood of patients with clinically diagnosed arteriosclerosis of blood vessels, not from healthy donors' blood.

Epigenomic studies call into question the legitimacy of extrapolating the interpretation of cellular responses in health to pathological conditions. Furthermore, contact cultivation of monocytes-macrophage with the material of implants *in vitro* will allow to evaluate individual features of cell interaction and to predict intravascular reactions to implants [18-21].

At the first stage of screening the choice of integral parameters for the assessment of cell-material interaction is crucial. The morpho-functional polarization of monocytes/macrophages (MN-MPh) can be used as their integral parameter. M1-polarization leads to the formation of a pro-inflammatory MPh phenotype with an elongated form and increased expression of CD40 and CD64. M2-polarization is associated with the formation of an anti-inflammatory MPh phenotype, where round-shaped cells express an elevated level of the mannose receptor and CD163. The dynamics of M1/M2 ratio was proved to play a key role in the pathogenesis of various diseases, in particular, of atherosclerosis [22-24].

In vitro and *in vivo* models allow controlling monocytes/macrophages polarization by various growth factors (M-CSF or GM-CSF), cytokines (IL-4, IL-10), IFN-γ/LPS, dexamethasone [25-27]. Another prospective approach is polarization control using biopolymer materials with various micro- and nano-relief through mechano-chemical signaling [28]. This type of signaling is associated with local changes in the curvature of the cell membrane in contact with the relief of the extracellular matrix or with the culture substrates or scaffolds. Membrane deformations alter the activity of membrane-bound proteins and trigger signaling process. Mechano-chemical signaling triggers the reorganization of the cytoskeleton and associated changes in cellular morphology. Furthermore, it is involved in the regulation of proliferation, differentiation, and apoptosis of cells [29-33].

This determines the important role of mechano-chemical signaling in the regulation of epigenetic rearrangements. Targeting regulatory signaling by features of micro- and nano-relief and transmission of topographic information into epigenome rearrangements is one of the most promising approaches in the development of polymeric materials for regenerative medicine, in particular, in technologies of development of bio-active vascular grafts, including vascular stents [34-35].

Therefore, our study focused on morphological aspects of the polarization of monocytes/macrophages, isolated from patients with atherosclerosis and on biodegradable polymeric materials of various compositions, promising for the production of vascular implants. We used the class of natural materials, polyhydroxyalkanoates (PHAs), with various monomeric compositions and different topography to assess the prospects of their application in intravascular stenting in patients with atherosclerosis.

Materials and Methods

Polyhydroxyalkanoate polymers (PHAs)

Samples of PHAs were obtained in the process of microbiological synthesis with the cultivation of Cupriavidus eutrophus B-10646 in specific growth conditions in the Laboratory of Biotechnology of New Materials, Siberian Federal University. Samples contained the following monomers: 3-hydroxybutirate, and 3-hydroxyvalerate, 4-hydroxybutyrate, 3-hydroxyhexanoate.

Biopolymer samples with the following composition were used in the study:

Sample 1: Poly-3-hydroxybutyrate [-O-CH(CH3)-CH_2-CO-], **P3HB**, scaffold 1.

Sample 2: Copolymers of 3-hydroxybutyrate and 3-hydroxyvalerate [-CH(C_2H_5)-CH_2-CO-], **P(3HB/3HV)**, scaffold 2.

Sample 3: Copolymers of 3-hydroxybutyrate and 4-hydroxybutyrate [-O-CH_2-CH_2-CH_2-CO-], **P(3HB/4HB)**, scaffold 3.

Sample 4: Copolymers of 3-hydroxybutyrate, 3-hydroxyvalerate and 3-hydroxyhexanoate [-O-CH-(C_3H_7)-CH_2-CO-], **P(3HB/3HV/3HH)**, scaffold 4.

Sample 5: Copolymers of 3-hydroxybutyrate, 3-hydroxyvalerate, 4-hydroxybutyrate and 3-hydroxyhexanoate [-O-CH(CH_3)-CH_2-CO-O-CH(C_2H_5)-CH_2-CO-O-(CH_2)$_3$-CO-O-CH(C_4H_9)-CH2-CO-O-], **P(3HB/3HV/4HB/3HHx)**; scaffold 5.

The molecular weight distribution of the samples was determined by gel permeation chromatography (Agilent Technologies, 1260 Infinity USA) with detection of the weight average and the number average molecular weight (Mw and Mn) and polydispersity PD. The thermal analysis of the samples was carried out using a differential scanning calorimeter DSC-1 (Mettler Toledo, Switzerland): melting point (Tmelt) and thermal degradation temperature (Tdegr) were found on the thermograms by using endothermic peaks, which were analyzed using the STARe v11.0 software (Mettler Toledo, Switzerland). Crystallinity (Cx) was determined using the diffractometer D8 ADVANCE (Bruker AXS, Germany) with a linear detector VANTEC.

Films were obtained by pouring polymer solutions in chloroform, followed by the solvent evaporation. Homogeneous solutions containing 10-20 g/l polymers were heated to 35°C and poured into the defatted surface of Petri dishes and dried for 2-3 days at room temperature in the laminar box; finally, films were dried to constant weight in a vacuum cabinet (Labconco, USA).

The surface characteristics of the films were evaluated using a contact angle measuring device DSA-25E (Kruss, Germany) using DSA-4 Windows software; the water contact angles were measured in the automatic mode; the video frame of the drop was processed in a semi-automatic mode after its stabilization by the "Circle" method built into the software package. The free surface energy, the polar component (mN/m) were calculated by Owens–Wendt–Rabel–Kaelble method using the obtained values of water contact angles. The scaffold surface microstructure was investigated by a scanning electron microscope. Samples with the size of 5 × 5 mm were preliminarily placed on a stage and sputtered with platinum using an Emitech K575X (Quorum Technologies Limited, UK); SEM images were obtained using TM (Hitachi, Japan). Surface roughness was determined using atomic force microscopy (AFM) in a semi-contact mode (Russia). The average (Ra) and the root-mean-square roughness (Rq) were calculated at 10 points

as the arithmetic average of the absolute values of the height deviations of the 5 highest and 5 deepest points from the midline of the profile using standard equations (Roughness parameters of the same name, ISO 4287/1). 20 × 20 μm sections were examined, then local maxima and minima 2 × 2 μm sections were selected and analyzed repeatedly with higher resolution, roughness for each sample was calculated for the three sections.

Patients

Patients of the Cardiology Centre in Krasnoyarsk, aged 60-70 and diagnosed coronary heart disease participated in the study. Studies were carried out with the permission of the Ethics Committee of the Cardiology Centre with the agreement, signed by participants. Prior to hospitalization, patients were prescribed traditional therapy for cardiac ischemia: acetylsalicylic acid, statins (atorvastatin or simvastatin), beta-blockers, calcium antagonists. Patients were prescribed clopidrogel 5 days prior to hospitalization.

One day after the hospitalization, transluminal balloon angioplasty was performed with 2nd-generation stents with everolimus (Promus Element plus, Boston Scientific Corporation, USA, or Xience Xpedition, ABBOT VASCULAR, USA). After the operation, patients were prescribed disaggregate therapy, statins, and beta-blockers.

Venous blood was twice collected from each patient (20 ml, anticoagulant – EDTA) the day before stenting and the day after stenting.

Monocyte isolation

Monocytes were isolated in the hypertonic density gradient of ficoll-verografin by the method of Recalde H [36]. The pre-prepared leukomass was layered on a hypertonic gradient (specific density 1,080 g/cm^3) and centrifuged at 400 g for 15 min. The monocyte fraction from the interphase was washed twice with phosphate buffer (pH = 7.0) (Amresco, USA) and centrifuged at 400 g for 10 min.

The cell concentration was determined in the Goryaev chamber. Cells were suspended in DMEM (Gibco, ThermoFisher Scientific, USA) with 10% fetal bovine serum (FBS) (HyClone, USA) and adjusted to 2 × 10^6 cells/ml (10^5 cells in 50 μl).

Polymeric films of different composition were placed in culture wells 96-well plates (TPP, Switzerland), then 100 μl of DMEM medium with 10% FBS and 50 μl of cell suspension (10^5 cells in each well) was added. Polystyrene culture plates served as control. The cells were cultured in a CO_2 incubator (New Brunswick Scientific Eppendorf, USA) for 6 days. Every 3 days the medium was changed. After finishing incubation MTT assay was performed and samples were prepared for morphological analysis using scanning electron microscopy.

MTT assay

At the end of the incubation, the culture medium was removed from the wells and the cells were washed with fresh DMEM medium with 10% FBS. 200 μl of MTT solution (Sigma-Aldrich, USA) in DMEM medium with 10% FBS (final MTT concentration of 0.25 mg/ml) was added to the wells. The cells were incubated for 4 hours. After the incubation, the medium was replaced by 150 μl of DMSO (Amresco, USA). Aliquots of 100 μl were transferred to clean plates and the optical density was determined at λ = 550 nm on a multichannel reader iMark™ Microplate Absorbance Reader (Bio-Rad, USA).

Scanning electron microscopy

After cell incubation, the culture medium was removed from the wells and the cells were fixed with 2.5% glutaraldehyde (Sigma-Aldrich, USA) in phosphate buffer (Amresco, USA) for 2 hours. The cells in the wells were additionally fixed with 1 % OsO_4 (SPI Supplies, Structure Probe, Inc., USA) for 40 min. After that biopolymer-cell samples were washed and passed through ethanol with increasing concentration (from 10% to 100% ethanol with step 10%). Biopolymer-cell samples were taken out of the wells. In the control variant, the bottom of the wells was cut out and fixed on aluminum foil or on metal object tables.

The samples were analyzed using scanning electron microscopy TM 3000 (Hitachi, Japan). Prior to microscopy the samples were sputter coated with platinum (3 cycles at 10 mA, for 20 s) with an Emitech K575X sputter coater (Quorum Technologies, England).

Statistics

Statistical analysis of the results was performed by conventional methods, using the Microsoft Excel software package. Arithmetic means and standard deviations were calculated. The statistical significance of results was determined using Student's test (significance level: $P \leq 0.05$). Statistical analysis of surface properties of the samples was performed by using embedded methods of the DSA-4 software.

Results

The basic physicochemical properties of polyhydroxyalkanoates

The five types of polyhydroxyalkanoate polymers, used for the films casting had different basic physicochemical properties.

Copolymers with the predominance of 3HB monomers, similar to P3HB homopolymer had similar melting points (162-160°C) and thermal degradation temperatures (268-273°C), as well as weight average molecular weight (1100 000-1200000 Da); the exception was the copolymer P(3HB/3HH) which had Mw values almost half the rest of the samples (Table 1).

One of the important biological characteristics of implants is the wettability of their surface by polar and nonpolar liquids which is determined by the value of the contact angle. A comprehensive assessment of both helps to predict the biocompatibility of material in direct contact with cells. The value of the contact angle of water wetting for the copolymer films was from 78, 65 to 97, 98 degrees with the minimum value for P (3HB/4HB); this is lower than for homo-polymer films (97.42) and control (92.46) which indicates a favourable effect of the monomers other than 3HB on the wettability. The P3HB homo-polymer films and the P (3HB/3HV/4HB/3HHx) copolymer films had the same wettability.

PHA composition (mol %)	Polymer characteristics				
	M_n, kDa	M_w, kDa	C_x, (%)	$T_{melt.}$ (°C)	$T_{degr.}$ (°C)
P3HB (100, 0)	657	1 200	74	167,6	273,8
P(3HB/3HV) (89,5/10,5)	220	695	59	173.2	283.5
P(3HB/4HB) (92/8)	580	1 100	42	162,2	268,4
P(3HB/3HV/3HHx) (66,4/23,4/10,2)	589	540	60	176	271
P(3HB/3HV/4HB/3HHx) (63,5/ 19,4/ 12,3 /4,8)	72	437	30	168	286

Table 1: Physicochemical properties of polymer samples (PHAs) used for the film production.

Surface roughness is the most important parameter for implantable biomaterials, determining the adhesion, spreading and motor activity of cells, the biosynthesis of specific proteins and mechano-chemical signalling. The study of the film surface roughness showed significant differences in film samples of different composition: height of the surface irregularities was significantly different from that of P3HB – the deviation of the roughness profile of the copolymers was almost 2.5 times higher than that of the homo-polymer. The root-mean-square roughness maximum was 248 nm in P (3HB/4HB); minimal value was 157 for a 4-component sample, with respect to 80 nm for P3HB (Figure 1 and Table 2).

Cell morphology on different culture substrates

Based on microscopic analysis of cells in different experimental conditions, two basic morphological classes were identified: 1 – rounded cells; 2 – elongated cells. Cells with unusual morphology (a small percentage of the cell population) were classified as class 3 (Table 3).

In the 1st morphological class two morphotypes were identified:

- rounded, single-nucleated cells.

- Large rounded cells with several nuclei.

In the 2nd morphological class four morphotypes were identified:

- Filamentous cells: strongly elongated cells, the length is many times greater than the transverse diameter.

- Spindle-shaped cells: elongated cells with spindle-shaped thickening in the middle of the cell body.

- Rod-shaped cells: elongated cells with the same transverse diameter throughout the cell body.

- Triangular cells: cells of triangular shape with one highly elongated apex.

Rounded form (the 1st morphological class) was referred to as stationary cells; elongated form (the 2nd morphological class) was referred to as mobile cells.

This classification was used to assess the morphological diversity of macrophages in control (culture plastic) and on PHA-biopolymer substrates of the different monomer composition.

MN-MPh culture on culture plastic

MPh obtained from MN, isolated before stent placement

On the 6th day of cultivation, the number of two main morphological classes of macrophages (rounded cells and elongated cells) was the same: 47.9% and 51.1% respectively. Among the rounded cells, relatively small single-nucleated cells predominated. In large rounded cells 2-3 nuclei were observed (Figure 2A-C).

They stood out as darkly rounded formations against the backdrop of numerous lipid droplets in the cytoplasm. Lipid drops in the cytoplasm were detected as numerous, very contrasting, nano sized vesicular structures. X-ray spectral analysis of cell samples showed that these vesicular structures colocalized with the sites of local concentration of osmium (Figure 3A-C).

OsO_4 is known to bind phospholipids in the region of the polar heads and interact with the double bonds of fatty acid residues in the lipids to form osmate esters [37]. This determines the concentration of osmium in the lipid droplets and their high contrast.

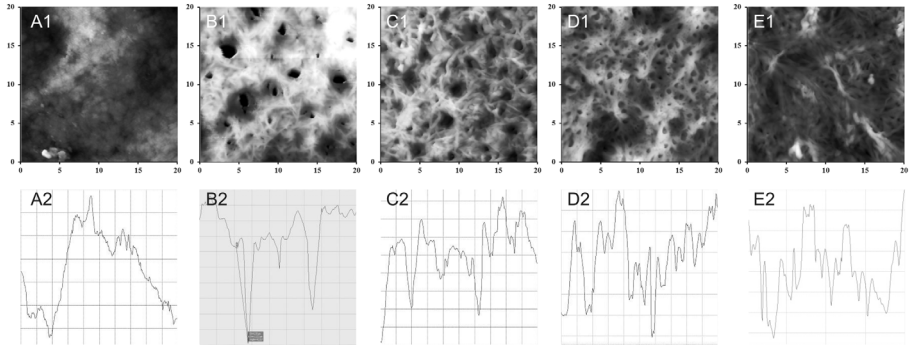

Figure 1: 3-D Surface topography of biopolymer scaffolds
A1 – E1 – 3-D reconstructions of the surface topography of scaffolds (surface areas 20 μm x 20 μm). A2 – E2 – cross-sectional profiles of the permanent topography of scaffolds. Abscissae axis is plane, 20 μm for all variants A2 – E2. Ordinates axis is the relief depth for A2 – [50 – 350 nm]; B2 – [400 – 2400 nm]; C2 – [100 – 900 nm]; D2 – [400 – 1100 nm]; E2 – [300 – 1000 nm]. A – P(3HB); B – P(3HB/4HB); C – P(3HB/3HV); D – P(3HB/3HV/3HHx) 66,4/23,4/10,2; E – P(3HB/3HV/4HB/3HHx) 63,5/ 19,4/ 12,3 /4,8. A – Scaffold 1; B – Scaffold 2; C – Scaffold 3; D – Scaffold 4; E – Scaffold 5.

PHA composition, (mol.%)	Water contact angle, (θ,°)	Surface free energy, (erg/cm^2)	Polar component of surface free energy, (erg/cm2)	Ra, Arithmetic mean surface roughness, (nm)	Rq, Root mean square roughness, (nm)	Rz, Height of the surface irregularities
P3HB	97,42 ± 2,6	30,43 ± 1,01	1,23 ± 0,18	71,75	80,28	184,03
P(3HB/3HV) (85,0/15,0)	88,00 ± 2,4	36,90 ± 0,24	2,40 ± 0,09	172,37	206,06	516,36
P(3HB/4HB)(92,0/8,0)	78,62 ± 1,2	44,52 ± 1,08	4,24 ± 0,14	177,56	248,10	1260,65
P(3HB/3HV/3HHx)(66,4/23,4/10,2)	89,80 ± 1,6	36,76 ± 1,10	1,90 ± 0,12	158,26	198,50	754,05
P(3HB/3HV/4HB/3HHx) (63,5/ 19,4/ 12,3 /4,8)	97,98 ± 1,9	25,82 ± 1,25	1,58 ± 0,42	120,91	157,54	728,63

Table 2: Surface properties of the films with different composition.

Experimental	Morphological classes, % of total cell number						
	Morphological class 1		Morphological class 2				Morphological class 3
	Rounded cells		Elongated cells				Cells with unusual morphology
	Morphotype 1	Morphotype 2	Morphotype 1	Morphotype 2	Morphotype 3	Morphotype 4	
	Multinuclear	Mononuclear	Filiform cells	Spindle-shaped cells	Rod-shaped cells	Triangular» cells	
Culture plastic, before stenting	19,75	28,18	3,50	26,75	5,73	15,13	0,96
Culture plastic, after stenting	19,10	35,76	1,04*	30,90	9,72*	3,13*	0,35*
Scaffold 1, before stenting	15,98	18,14	6,26	43,20	9,94	2,59	3,89
Scaffold 1, after stenting	20,49	22,97	9,19*	33,22	6,01*	1,77*	6,36*
Scaffold 2, before stenting	10,87	54,35	1,09	23,91*	3,26	3,26	3,26
Scaffold 2, after stenting	11,51	9,47*	17,99*	50,00	6,24*	0	2,52
Scaffold 3, before stenting	9,30	46,51	3,10	30,23	5,43	4,65	0,78
Scaffold 3, after stenting	4,17*	37,50	4,17	41,67	8,33*	4,17	0,00
Scaffold 4, before stenting	14,98	20,70*	8,81	36,56	10,57	6,17	2,20
Scaffold 4, after stenting	5,45*	13,64	3,64*	60,91*	6,36*	7,27	2,73
Scaffold 5, before stenting	10,48	31,43	3,81	37,14	11,43	5,71	10,48
Scaffold 5, after stenting	17,74	40,32	4,84	29,03	3,23*	3,23*	1,61*

Note: An asterisk indicates the cases where the value after the stent installation (before stenting) was significantly different from the value before the stent installation (after stenting) ($p \leq 0.05$).

Table 3: Morphological classes and morphotypes of MPh on the 6th day of cultivation on standard culture plastics and biopolymer scaffolds of various composition. MNs were isolated from the patient's blood before the stent was installed and after the stent was installed. MNs were cultivated on culture plastic and on biopolymers scaffolds of various compositions (scaffolds 1, 2, 3, 4, 5) in 96-well culture plates (10^5 cells/well) in DMEM medium with 10% fetal serum in CO_2-incubator. After 6 days of culture, the cells were fixed in the wells of the plate with 2.5% glutaraldehyde and samples were prepared for electron microscopy using a standard protocol.

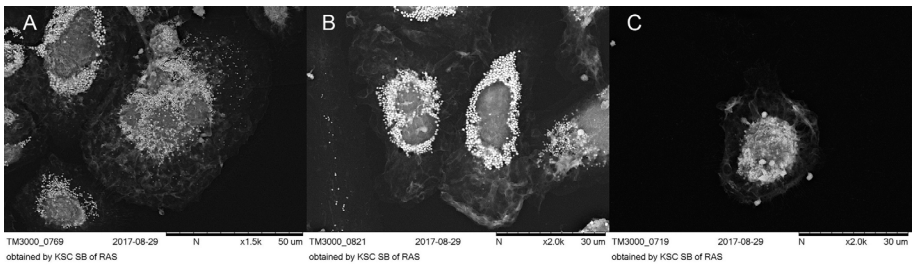

Figure 2: Morphotypes of the 1st morphological class. 6 days, culture plastic. A, B – morphotype of multinuclear cells. Large cells with numerous lipid droplets in the cytoplasm. Nuclei are seen as gray, rounded structures against the background of high-contrast lipid droplets. C – morphotype of mononuclear cells. Both morphotypes have a complex relief of the plasma membrane.

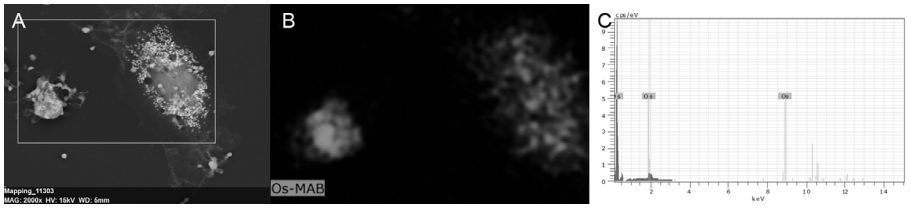

Figure 3: X-ray spectral analysis of macrophages. A – area selected for analysis. B – the area of osmium localization (red zones). C - Characteristic spectral lines of osmium.

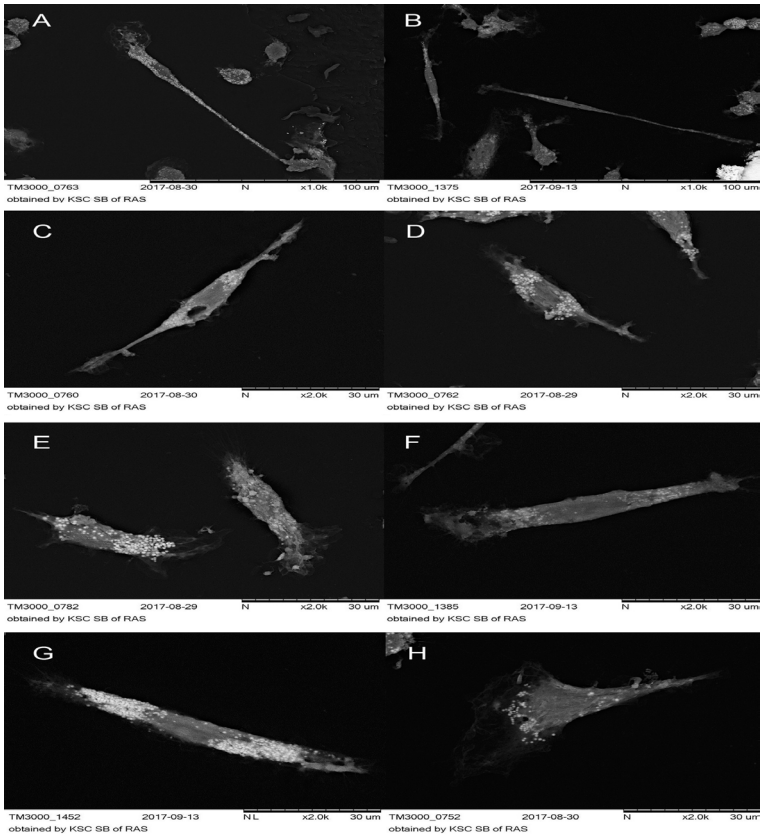

Figure 4: Morphotypes of the 2nd morphological class. 6 days, culture plastic. A, B - morphotype of filamentous cells; long, "thin" cells, the length varies from 80 microns to 150 microns (indicated by white arrows). C, D - morphotype of spindle-shaped cells; relatively "short" cells with a pronounced central spindle-shaped thickening. E, F, G - morphotype of rod-shaped cells; elongated cells of approximately the same diameter along the entire length. F - morphotype of triangular cells. Lamellopodia with complex surface relief of the plasma membrane, located at the poles were observed for all 4 morphotypes. Magnification: x1000 (A, B), x2000 (C, D, E, F).

In the morphological class of elongated cells, two morphotypes dominated: spindle-shaped cells (26.75%) and triangular cells (15.13%) (Figure 4A-H).

MPh obtained from MN, isolated after stent placement

In this experimental condition on the 6th day of cultivation, the number of basic morphological classes (rounded and elongated cells) did not differ significantly from the variant before stent placement. Based on this it can be assumed that stent placement did not affect the number of mobile cells *in vitro*. But the relationship between the morphotypes in each morphological class changed radically after the stent was installed.

In the morphological class of elongated cells, the number of filamentous and triangular cells decreased by 3.5 and 3 times respectively, and the number of rod-shaped cells increased by 1.7 times as compared with before stent placement (Table 3).

In the morphological class of rounded cells, the percentage of the multinucleated cells did not change (in comparison with the variant before the stent was installed). But the ratio between the two morphotypes shifted strongly toward mononuclear cells: the number of multinucleated cells was 1.9 times lower than single nucleated cells (this ratio was 1.4 before stent placement).

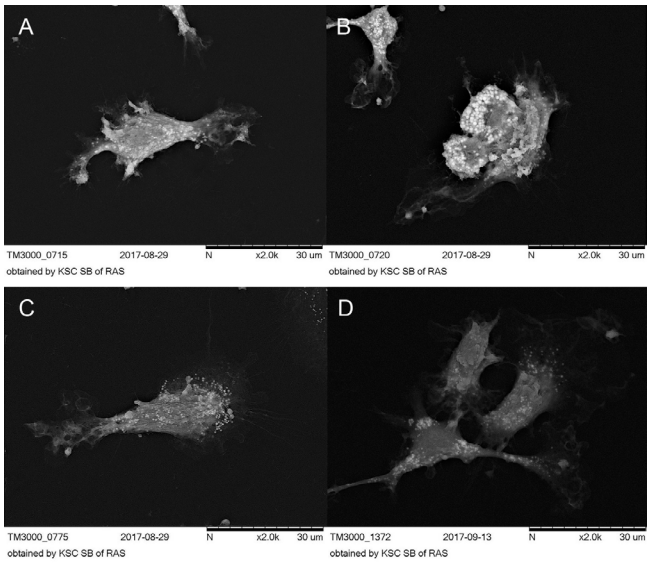

Figure 5: Morphotypes of the 3rd morphological class (unusual morphology). 6 days, culture plastic. A, B, C, D – variants of the 3rd morphological class morphotypes.

The 3rd morphological class with indefinite morphology was not numerous when cultivated on plastics both before and after stenting and was low than 1% (Figure 5A-D).

Complicated membranous relief in the periphery of round cells and lamellipodia of cells of 2nd and 3rd morphological classes were MPh characteristic on culture plastic. The lamellipodia of morphotypes of filamentous cells had the form of round-shaped pad flat leg (Figure 6A-F).

MC-MPh culture on biopolymer scaffolds

The analysis of the surface of biopolymer scaffolds using scanning microscopy revealed a complex micro-nanoscale relief, which was formed during the drying of a polymer film.

The surface relief of the polymer samples varied depending on the monomeric composition. The relief of the scaffolds 1 and 4 was more "coarse" and loose with large deep pores. The surface relief of the scaffolds 2, 3 and 5 was more "delicate", resembling small ripples on the water surface. The relief of the scaffold 5 was characterized by small numerous pores (Figure 7A-E).

Morphological analysis of MPh on biopolymer scaffolds with various micro/nano reliefs revealed 3 main morphological classes, which were also observed during cell cultivation on culture plastics. So, for example, a morphotype of spindle-shaped cells (the second morphological class) (Figure 8A-E), which was observed on all samples

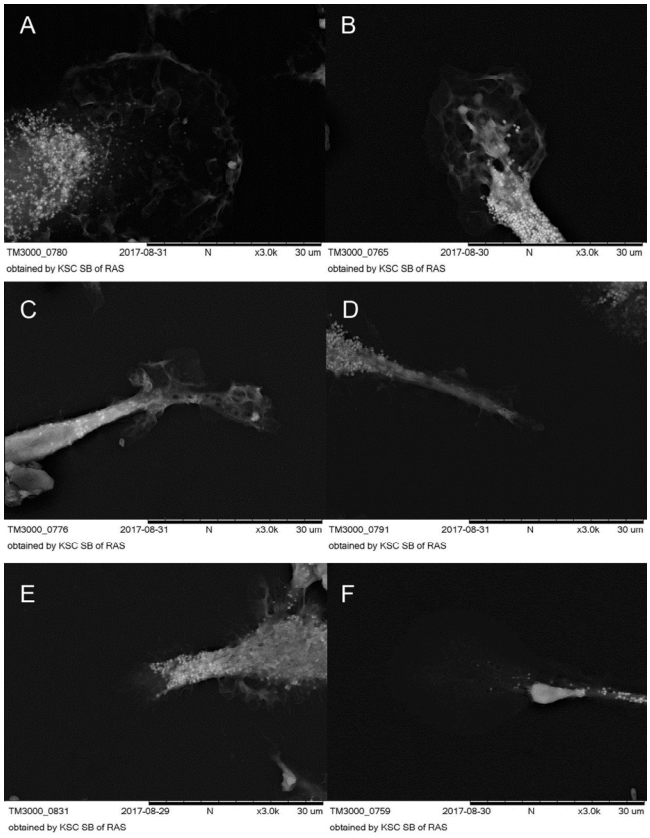

Figure 6: Morphology of macrophage lamellopodia on culture plastic. A – lamellopodia of the 1st morphological class cells. B, C, D, E, F – lamellopodia of the 2nd morphological class cells. F – a rounded paw lamellopodia typical for the morphotype of filamentous cells.

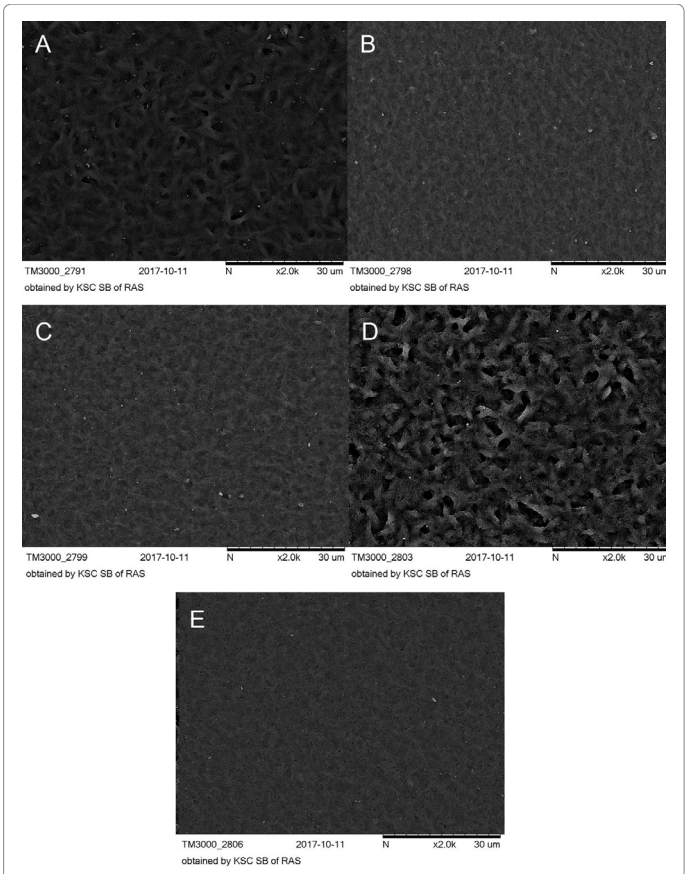

Figure 7: Surface microrelief of the of biopolymer scaffolds of various compositions (Table 1). A - Scaffold 1; B - Scaffold 2; C - Scaffold 3; D - Scaffold 4; E - Scaffold 5.

was also encountered among the MPh on culture plastics. Large round multinucleate cells (the 1st morphotype of the 1st morphological class) were observed on all biopolymer substrates, but on the substrate 5, these cells reached enormous sizes (Figure 9A-E).

It should be noted, that the complex membranous relief along the periphery of rounded cells and lamellopodia of cells of the 2nd and 3rd morphological classes, which was characteristic for the results on the culture plastics, was significantly "simplified" on biopolymer scaffolds (Figure 10A and 10B).

The same MPh morphotypes were detected on culture plastic and on biopolymer substrates, but the quantitative relationships between different morphotypes varied significantly depending on the characteristics of the micro/nano relief of the sample surface and on MN release option – before and after stent placement.

On the basis of the morphological analysis, several parameters were selected for an integral evaluation of the macrophage morphology in different samples.

The ratio between the number of the 1st and 2nd morphological classes (the ratio between the number of rounded and elongated cellular forms), $\mathbf{K}_{M1/M2}$ (Figure 11).

This parameter varied significantly depending on the type of substrate and time of cell isolation, i.e. whether isolated before or after stent installation. For the cells, isolated before the stenting the

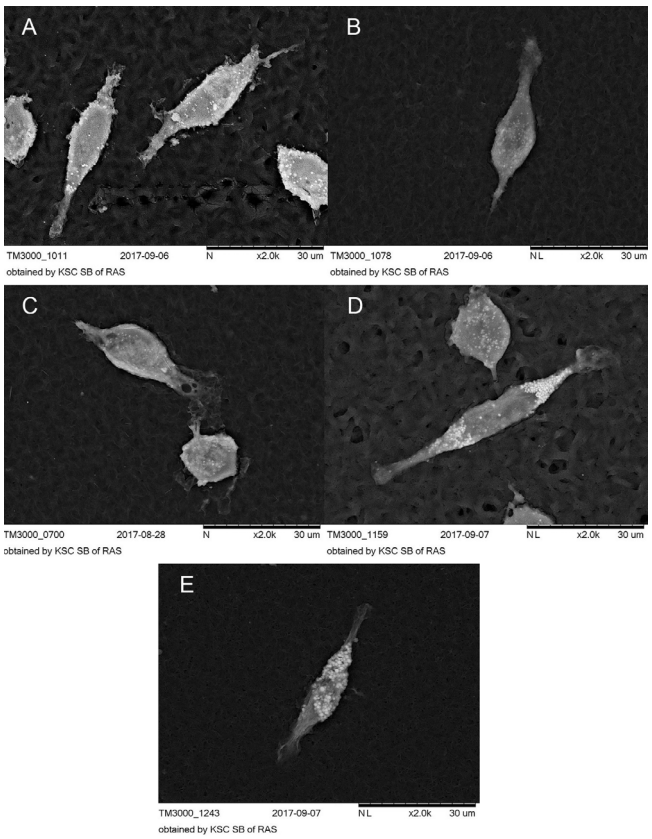

Figure 8: Morphotype of spindle-shaped cells (2nd morphological class) on biopolymer scaffolds of different composition. A – scaffold 1; B – scaffold 2; C – scaffold 3; D – scaffold 4; E – scaffold 5.

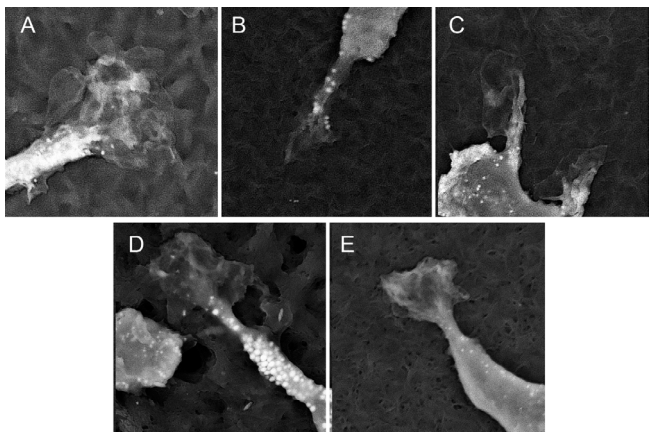

Figure 9: Morphology of MPh lamellopodia on biopolymer scaffolds of different composition. A - Scaffold 1; B - Scaffold 2; C - Scaffold 3; D - Scaffold 4; E - Scaffold 5.

parameter value decreased as follows: **Scaffold 2 (2.07) > Scaffold 3 (1.29) > Plastic (0.94) > Scaffold 5 (0.72) > Scaffold 4 (0.57) > Scaffold 1 (0.55).**

For the cells, isolated after the stent installation this parameter value decreased in an absolutely different way: **Scaffold 5 (1.44) > Plastic (1.22) > Scaffold 1 (0.87) > Scaffold 3 (0.71) > Scaffold 4 (0.24) > Scaffold 4 (0.24).**

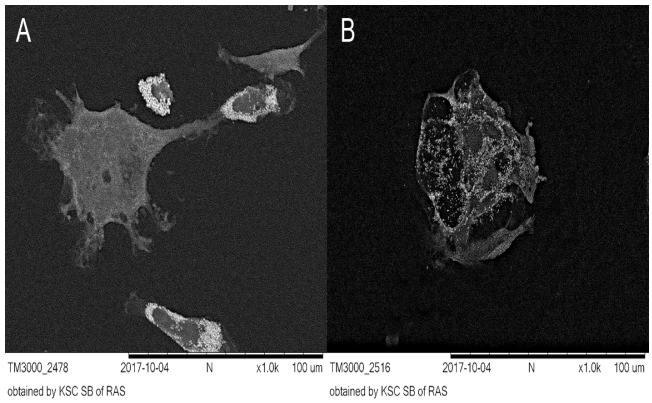

Figure 10: Giant multinuclear cells on the biopolymer scaffold. A - Neuron-like cell with lamellopodia; B - A rounded cell with a lot of lipid droplets in the cytoplasm.

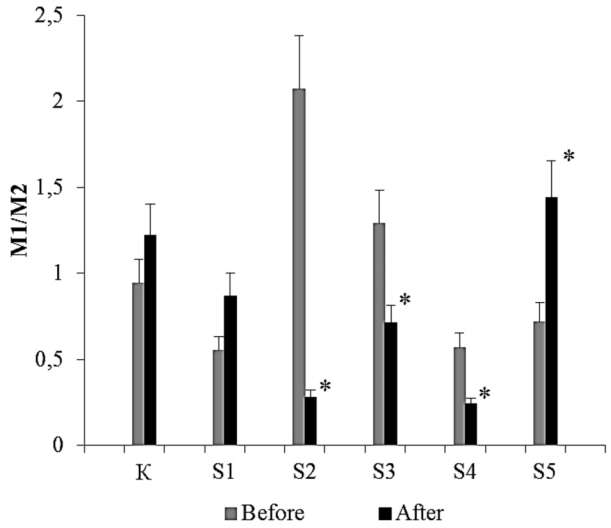

Figure 11: The ratio between the cell number of the 1st and the 2nd morphological classes (M1/M2-phenotypes) on the 6th day on culture plastic and biopolymer scaffolds before (Before) and after (After) stenting. M1 – rounded cells, M2 – elongated cells.
Abscissae axis: K – culture plastic; S1 – scaffold 1; S2 – scaffold 2; S3 – scaffold 3; S4 – scaffold 4; S5 – scaffold 5. An asterisk indicates the cases where the value after the stent installation (After) was significantly different from the value before the stent installation (Before) ($p \leq 0.05$).

It should be noted, that during cell cultivation on standard culture plastics the value of $\mathbf{K}_{M1/M2}$ did not differ significantly in the culture variants before and after stent placement. For the culture on biopolymer scaffolds of different composition, the value of $\mathbf{K}_{M1/M2}$ was significantly different for variants before and after stent implantations. Moreover, the direction of $\mathbf{K}_{M1/M2}$ variation was not the same for biopolymer scaffolds of the different monomer composition. After stenting $\mathbf{K}_{M1/M2}$ for the scaffolds, 1 and 5 increased, for scaffolds 2, 3, and 4 – decreased if compared with the variant before stenting.

The ratio between the number of 2nd and 1st morphotypes in the 1st morphological class (the ratio between the number of mononuclear (MOC) and multinucleated (MUC) cells) KMOC/MUC (Figure 12).

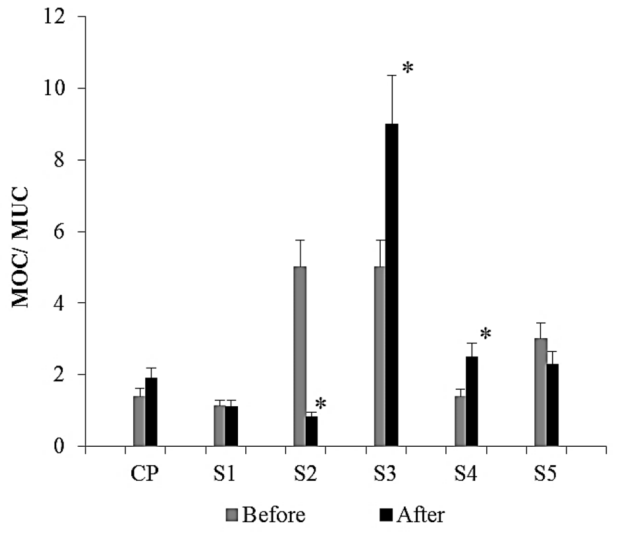

Figure 12: The ratio between the rounded mononuclear cells (MOC) and rounded multinuclear cells (MUC) (1st morphological class) on the 6th day on culture plastic and biopolymer scaffolds before and after stenting. Abscissae axis: K – culture plastic; S1 – scaffold 1; S2 – scaffold 2; S3 – scaffold 3; S4 – scaffold 4; S5 – scaffold 5. An asterisk indicates the cases where the value after the stent installation (After) was significantly different from the value before the stent installation (Before) ($p \leq 0.05$).

Variability of this parameter was significantly higher than the $\mathbf{K}_{MOC/MUC}$ parameter and depended on scaffold type and isolation time.

For the cells isolated before stent installation the value of $\mathbf{K}_{MOC/MUC}$ decreased as follows: **Scaffold 2 (5.00) = Scaffold 3 (5.00) > Scaffold 5 (3.00) > Plastic (1.40) > Scaffold 4 (1.38) > Scaffold 1 (1.13).**

For the cells isolated after stent placement the value of this parameter decreased differently: **Scaffold 3 (9.00) > Scaffold 4 (2.50) > Scaffold 5 (2.30) > Plastic (1.90) > Scaffold 1 (1.12) > Scaffold 2 (0.82).**

The change direction in $\mathbf{K}_{MOC/MUC}$ was not the same for biopolymer scaffolds of different composition. After stenting $\mathbf{K}_{MOC/MUC}$ for culture plastic scaffolds 3 and 4 increased, for scaffolds 2 and 5 decreased, compared with the variant before stenting. For scaffolds 1 $\mathbf{K}_{MOC/MUC}$ was the same before and after stenting.

For cultural plastic and various variants of biopolymer scaffolds, specific ratio between the parameters $\mathbf{K}_{M1/M2}$ and $\mathbf{K}_{MOC/MUC}$ depended on cultivation variant before or after stenting. At the same time, it should be noted that the variability of the parameters of $\mathbf{K}_{M1/M2}$ and $\mathbf{K}_{MOC/MUC}$ was significantly higher for biopolymer scaffolds than for culture plastic. This allows us to consider such system as more promising for change assessment in MPh functional state *in vivo* (vascular bed), based on changes in the differentiation processes of Mn to MPh *in vitro*.

MTT reduction activity in macrophages in various culture conditions

MTT test is based on the intracellular reduction of the water-soluble tetrazolium dye MTT into insoluble formazan with the participation of NAD (P) H-dependent oxidoreductases. Formazan formation depends on the availability of NAD (P) H and can serve as an integral measure of the activity of NAD(P)H production and the activity of NAD(P) H-dependent metabolic cycles [36-39]. NAD (P) H is known to play an important role in the epigenetic and metabolic reprogramming of macrophages (differentiation and polarization processes) [40-42]. In this connection, the activity of MTT reduction to formazan was determined under different culture conditions (Table 4).

It was shown that in the case of MN isolation before stent installation MTT reduction activity on scaffolds 2 and 3 was 1.5 times less if compared to culture plastic. In the case of MN isolation after the stent was installed MTT reduction activity on the scaffold 4 was 1.5 times higher than that on culture plastic. These features were revealed for MTT reduction activity, expressed as a percentage of the control group (culture plastic). The analysis of the absolute values of optical density made it possible to reveal additional patterns. After stent installation, the MTT reduction activity on culture plastic and on the scaffold 1 decreased 1.7 times if compared with the corresponding values for the variant before stent placement (Table 4). There were no significant differences in the activity of MTT reduction in formazan between variants before and after stent placement on scaffolds 2, 3, 4, and 5.

It should be noted that at the cellular level the variability of morphotypes under different culture conditions was more significant than the variability of MTT reduction activity.

Discussion

The reason for such a diversity of Mph morphotypes *in vitro* may be the heterogeneity of monocytes circulating in the blood *in vivo* [43-46]. By the nature of expression of surface antigens, three subpopulations of circulating MN are isolated: CD14++CD16--classic Mn1, CD14++CD16+-interim Mn2, and CD14+CD16++-Mn3, non-classical. But it is possible to "divide" MN into various subpopulations using other surface antigens [47].

Subpopulations are characterized by differential expression of the genes that determine their specific functions and implications for physiological and pathogenic processes [46,47]. Specific MN subpopulations control the structural and functional integrity of the vascular endothelium, activity of infiltration of neutrophils in tissues. Certain MN subpopulations leave the vascular bed and patrol the extracellular space of various organs and tissues and return back to the bloodstream (possibly in another morphological and functional status state) [48-53]. For such pathology as atherosclerosis, the active yield of MPh-foam cells from the body of an atherosclerotic plaque is considered as one of the approaches to targeting this disease. It is possible, that different MN subpopulations give rise to specific MPh subpopulations and dendritic cells in tissues and organs [54].

MPh subpopulation is a labile system, the number and functional activity of which can vary considerably in terms of physiological norm and pathogenesis [55]. There is a reason to believe that subpopulations of circulating MN are different stages of cellular differentiation [56], which may be modified under the influence of various factors.

Stent placement is a surgical procedure, associated with a relatively small loss of blood, but with the tangible intervention into a vessel. Even this insignificant blood loss can provoke the release of a fresh portion of monocytes from the bone marrow. On the other hand, an X-ray contrast substance is introduced to conduct stenting in the bloodstream, which can affect the functional state of circulating MN. Finally, being a fairly rigid mechanical structure, the stent in the delivering system can damage the endothelium of intact parts of the vascular wall, endothelium in the zone of plaque and the body of the plaque itself. As a result, in the focused zone the local gradient of cell

MN isolation	Scaffolds					
	S1	S2	S3	S4	S5	CP
Before	116%	63%	68%	98%	82%	100%
	(0,405)	(0,220)*	(0,237)*	(0,338)	(0,284)	(0,348)
After	118%	92%	119%	149%	109%	100%
	(0,232)#	(0,180)	(0,233)	(0,293)*	(0,214)	(0,196)#

Note: Asterisk * indicates the values significantly different from the values for culture plastic (CP) ($p \leq 0.05$) for each variant of MN isolation (before or after stenting). The # icon indicates the values for the MN isolated after the stent installation (After) significantly different from the values for the MN isolated before the stent installation (Before) ($p \leq 0.05$).

Table 4: MTT assay: the activity of MTT reduction to formazan in various cultivation conditions. MNs were isolated from the patient's blood before the stent was installed (Before) and after the stent was installed (After). MNs were cultured on culture plastic (CP) and on the biopolymer scaffolds of various compositions (S1, S2, S3, S4, S5) in 96-well culture plates (10^5 cells/well) in DMEM medium with 10% fetal serum in a CO_2 incubator. After 6 days of culture, the activity of MTT reduction to formazan was determined. MTT assay results were presented in % of control (culture plastic, 100%). The activity of MTT reduction is presented as an optical density at λ = 550 nm in parentheses, under percentages.

degradation products may accumulate. These are chemical signals which can affect the zone passing through the stent MN. Ultimately, by the time of resampling of blood from a patient in a day after the stent placement circulating MN (the ratio of different subpopulations of functional phenotypes, i.e., structural and functional heterogeneity) may differ significantly from MN, isolated from the patient's blood before the stent placement.

We must assume that the structural and functional heterogeneity of MN in vivo determines the characteristics of interaction with cell anchorage and morphotypes diversity in cell culture scaffolds *in vitro*. It is known, that changes in the morphology of cells, nuclei and cell organelles may trigger signaling system of metabolic and epigenetic reprogramming in cells (mechanochemical signaling) [34-35,56-59]. And in this connection, the analysis of cellular morphotypes can be useful at the stage of screening cultural substrates of various compositions for the presence of "reprogramming" activity.

It was shown, that the functional M1-M2 polarization in MPh *in vitro* is associated with cell morphology: rounded MPh fall into the M1-phenotype (proinflammatory MF), MPh with the elongate shape – to the M2 phenotype (MPh, involved in repair processes) [60,61]. Based on the morphological characteristics (the ratio of the number of 1st and 2nd morphological classes, rounded and elongated cells, Table 3), we can conclude, that before the stent installation in the process of MPh differentiation and polarization on culture plastic the ratio of cell populations with M1 and M2 phenotype was the same (M1/M2=0.94). After stent placement, the ratio of M1 and M2 phenotypes did not change significantly (M1/M2=1.22), but it became slightly higher.

Among the rounded cells (the 1st morphological class), large multinuclear MPh were observed as the fusion result of several mononuclear cells (Figures 2 and 9). The process of cell fusion is a cellular reaction of MPh, which is triggered, in particular, by the interaction with the implant material (giant multinuclear cells *in vivo*) [62,63]. It is assumed, that the interaction of MPh with highly curved surfaces triggers the processes of cell fusion (possibly via the system of mechanochemical signaling). One such an example is multinuclear osteoclasts, MPh of bone tissue, "working" with such surface type. It is assumed, that the giant multinuclear MPh may also be subjected to the M1-M2-polarization and their round shape is not always indicative of M1 phenotype [64].

Before and after stent placement the total number of multinuclear MPh on culture plastics was the same (19%), i.e. the activity of the fusion reaction of mononuclear MPh on the culture plastic surface after the stent installation procedure did not change. However, the ratio between multinuclear and mononuclear MPh after stent placement shifted toward mononuclear cells: the number of multinuclear cells was 1.9 times less than the number of mononuclear cells. Before the stent installation. This ratio was 1.4 (Figure 12).

Statistically significant changes in the ratio of the number of M1 and M2 phenotypes, rounded and elongated cells, i.e. changes in the direction of the processes of MPh polarization on culture plastics before and after stent placement were not observed. However, this may be not due to the absence of changes in the MN population, and accordingly, to the differentiation and polarization processes of MPh after stent placement, but to the peculiarities of culture plastic, that do not allow to reveal these changes at the morphological level.

This assumption is confirmed by the morphological analysis of MPh before and after stent placement during cultivation on biopolymer scaffolds with different composition: the stent installation procedure has a significant effect on functional phenotypes of circulating MN *in vivo* and resulted in significantly modified differentiation and polarization of MPh *in vitro*.

Quantitative changes in the ratio of different MPh morphotypes before and after stenting were expressed to a much greater extent on biopolymer scaffolds than on culture plastics (Figure 13A-F).

Based on changes in the number of M1-M2 phenotypes we can say that the biopolymer scaffolds may affect the processes of polarization of MPh *in vitro* and this influence is determined by the monomer composition and micro/nano relief of the scaffolds. And the polarization direction of MPh *in vitro* at the same biopolymer scaffolds also depends on the initial functional state of MN *in vivo* at the time of the isolation of these cells (Figure 11). It can be assumed, that in 24 hours after the stent installation new structural and functional phenotypes were formed in the Mn population of the vascular bed. It determines the development of new "relationships" of cells with the biopolymer scaffolds and, accordingly, specific variants of differentiation and polarization of MPh *in vitro*. This is an important fact not only for screening in the systems *in vitro*. Stenting as the surgical procedure and the foreign body can provoke 'aggressive' behaviour of the MN and the formation of "hot points" in the zones of stenting, which may disturb the process of re-endothelization of the stent to activate the proliferation of smooth muscle cells and ultimately lead to restenosis.

Along with the variability of MPh polarization processes, one should note the variability of the number of multinuclear MPh forms. The number of these cells also depends on the composition of the biopolymer scaffolds and on the variant of obtaining MN – before or after the stenting. So, on the sample scaffold 5 the number of multinuclear forms of MPh increased after stenting, and on scaffolds

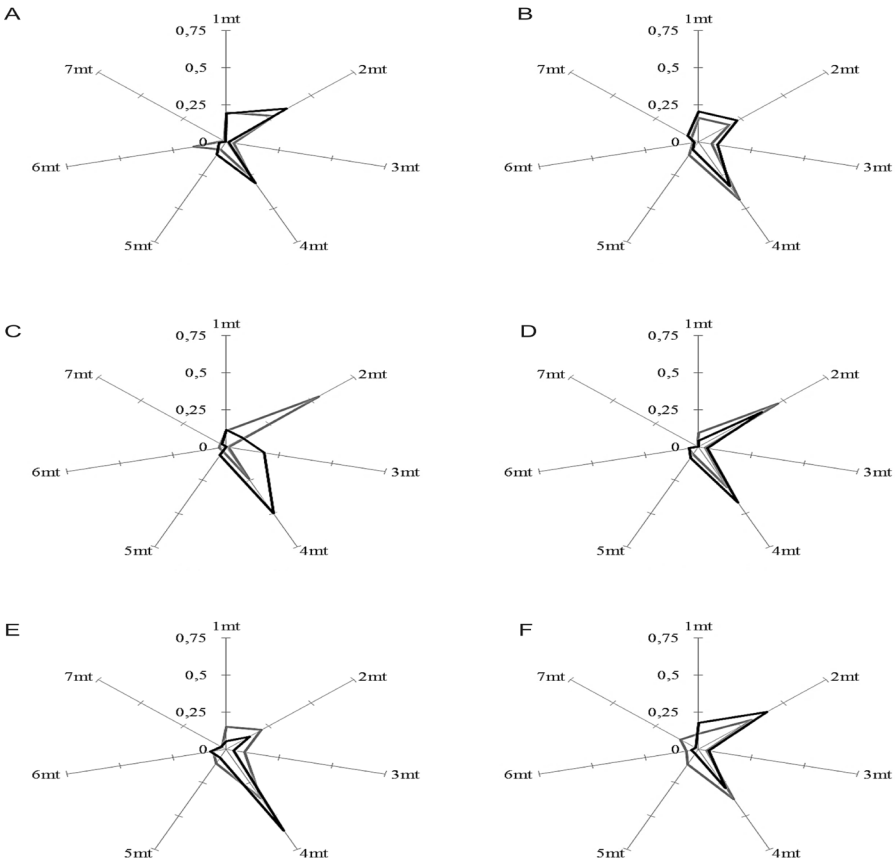

Figure 13: The ratio of different morphotypes (mt) on the 6th day on culture plastic and biopolymer scaffolds of different composition before (Before) and after (After) stent installation. A - culture plastic; B - scaffold 1; C - scaffold 2; D - scaffold 3; E - scaffold 4; F - scaffold 5. 1mt - the morphotype of multinucleated cells; 2mt - morphotype of rounded single nucleated cells; 3mt - morphotype of filamentous cells; 4mt - morphotype of spindle-shaped cells; 5mt - morphotype rod-shaped cells; 6mt - morphotype of "triangular" cells; 7mt - morphotype of a cells with unusual morphology.

3 and 4 – it decreased if compared with the variant before stenting. In substrates 1 and 2 and in control of culture plastics, the number of multinuclear MPh before and after stenting was the same (Table 3 and Figure 12).

Formation of multinuclear cells is the cell adaptation, aimed at improving the efficiency of degradation of foreign materials with a large radius of curvature [64]. It can be assumed, that the different number of multinuclear MPh under different cultivation conditions can determine the biodegradability of biopolymers, used for the production of experimental scaffolds. And the dynamics of biodegradation is determined not only by biopolymer properties but also by the variability of the processes of differentiation and polarization of MPh.

As already mentioned, it is customary to refer elongated cells to M2-MPh. In this morphological class various quantitative relationships between these four different morphotypes were formed on different biopolymer scaffolds before and after stenting. In general, the morphology of these cells indicates their mobility and active movement along the substrate. It is possible, that these are different subpopulations of MPh with different molecular "ways" of locomotion. Different types of locomotor behavior were demonstrated on a monolayer of endothelial cells *in vitro* for different MN subpopulations (classic CD14++CD16-, intermediate CD14++CD16+, and not-classical CD14+CD16++). These differences in locomotor behavior of MN subpopulations were associated with different adhesion molecules [65].

It is possible, that the variability in the number of mobile morphotypes of MPh can also be related to the features of substrate relief. The smooth surface of the culture plastic and the complex relief of the biopolymer scaffolds determine the different activity of the cell adhesion processes, locomotion machinery, and cell morphology, as a result. Moreover, it should be noted, that not only the relief structure determines the locomotion machinery, but the features of the functional phenotype of MPh can form different types of locomotor behavior of cells on the same biopolymer scaffold. Thus, on the biopolymer scaffold 2, after the stent was installed, the number of the morphotype of the filamentous cells increased 18-fold, compared with the variant before the stent was installed.

MPh polarization, along with morphological changes, is associated with metabolic reprogramming. The pentose phosphate pathway (or hexose-monophosphate shunt) is the key metabolic pathway which the direction of MPh polarization depends on. Hexose monophosphate shunt is the main metabolic pathway, generating NADPH. The M1-polarization process is associated with the direction of the glucose flow into the hexose-monophosphate shunt and the increase in NADPH production [40,66]. NADPH as an energy equivalent uses

various oxidoreductases, producing reactive oxygen species, which are included in the processes of epigenetic reprogramming of MPh [67]. In M2-MPh glucose flux in the hexose monophosphate shunt is limited, and NADPH synthesis activity drops sharply [66].

I.e., in the first approximation, we can assume that the high level of NADPH production in M1-MPh can identify and recover a high activity of MTT reduction in formazan by NADPH-oxidoreductases. The variability of MTT reduction activity in formazan can depend on the ratio of M1/M2 phenotypes. However, the correlation analysis did not reveal reliable correlations between these two parameters.

In general, the variability of MTT reduction activity was insignificant for various cultivation options (compared to the variability of cellular morphotypes). This integral parameter of the metabolic activity of cells is not demonstrative for the primary screening of the reprogramming activity of biopolymer scaffolds.

The results show the effectiveness of the primary screening reprogramming activity of biopolymers (as potential materials for vascular stents) on the basis of morphological analysis of MPh-culture *in vitro*. Based on the obtained results, samples of biopolymers will be selected for further study of the cellular polarization processes of MPh with the use of specific markers.

Conclusion

We determined 3 morphological classes of MN-MPh during the cultivation of cells of patients with atherosclerosis:

1st morphological class – rounded cells (M1-phenotype) which have 2 morphotypes: mononuclear and multinuclear cells;

The 2nd morphological class is elongated cells (M2 phenotype) which have 4 morphotypes: filiform, spindle-shaped, rod-shaped and triangular cells;

3rd morphological class – cells of unusual shape.

The proportion of morphotypes in the MPh cell population depends on the profile of the contact surface of the sample of PHAs and on its monomer composition. The procedure of stenting also affects the ratio of MPh morphotypes. The number of multinuclear cells on PHAs-samples of different compositions may indicate the activity of polymers biodegradation, similarly to the process of formation of giant cells of foreign bodies *in vivo*.

The obtained results demonstrate the dependence of the biological activity of biodegradable polymer scaffolds of different compositions not only on the specificity of the micro/nano relief of their surface but also on the features of the initial structural-functional state of MN blood population in patients before and after the intervention. Specific ratios of MPh morphotypes adequately reflect the interaction of surface relief and functional phenotype of cells *in vitro*, and this ability may be useful for screening biomaterials for vascular stenting and for effective monitoring of molecular-cellular events in the stenting area in patients after stenting procedure. The surface profile of the material affects the polarization processes and has the ability to trigger the systems of mechano-chemical signaling and subsequent reprogramming of metabolism, reorganization of the cytoskeleton and cell epigenome.

Acknowledgement

The study was supported by the State budget allocated to the fundamental research at the Russian Academy of Sciences (project No 01201351505).

References

1. Le Borgne M, Caligiuri G, Nicoletti A (2015) Once upon a time: the adaptive immune response in atherosclerosis – A fairy tale no more. Mol Med 21: 13-18.
2. Zaina S, Lund G (2017) Connecting the dots between fatty acids, mitochondrial function, and DNA methylation in atherosclerosis. Curr Atheroscler Rep 19: 36.
3. Yang X, Li Y, Li Y, Ren X, Zhang X, et al. (2017) Oxidative stress-mediated atherosclerosis:Mechanisms and therapies. Front Physiol 8: 600.
4. Zmysłowski A, Szterk A (2017) Current knowledge on the mechanism of atherosclerosis and pro-atherosclerotic properties of oxysterols. Lipids Health Dis 16: 188.
5. Gaudet D, Drouin-Chartier JP, Couture P (2017) Lipid metabolism and emerging targets for lipid-lowering therapy. Can J Cardiol 33: 872-882.
6. Rahman MS, Woollard K. Atherosclerosis (2017) Adv Exp Med Biol 1003: 121-144.
7. Groh L, Keating ST, Joosten LA, Netea MG, Riksen NP (2018) Monocyte and macrophage immunometabolism in atherosclerosis. Semin Immunopathol 40: 203-214.
8. Block T, El-Osta A (2017) Epigenetic programming, early life nutrition and the risk of metabolic disease. Atherosclerosis 266: 31-40.
9. Jia SJ, Gao KQ, Zhao M (2017) Epigenetic regulation in monocyte/macrophage: A key player during atherosclerosis. Cardiovasc Ther 35: e12262.
10. Khyzha N, Alizada A, Wilson MD, Fish JE (2017) Epigenetics of atherosclerosis: emerging mechanisms and methods. Trends Mol Med 23: 332-347.
11. Kolodgie FD, Yahagi K, Mori H, Romero ME, Hugh H, et al. (2017) High-risk carotid plaque: lessons learned from histopathology. Semin Vasc Surg 30: 31-43.
12. Bories GF, Leitinger N (2017) Macrophage metabolism in atherosclerosis. FEBS Lett 591: 3042-3060.
13. Panh L, Lairez O, Ruidavets JB, Galinier M, Carrie D, et al. (2017) Coronary artery calcification: From crystal to plaque rupture. Arch Cardiovasc Dis 110: 550-561.
14. Kowara M, Cudnoch JA, Opolski G, Wlodarski P (2017) MicroRNA regulation of extracellular matrix components in the process of atherosclerotic plaque destabilization. Clin Exp Pharmacol Physiol 44: 711-718.
15. Brancati MF, Burzotta F, Trani C, Leonzi O, Cuccia C, et al. (2017) Coronary stents and vascular response to implantation: literature review. Pragmat Obs Res 8: 137-148.
16. Nakamura K, Keating JH, Edelman ER (2016) Pathology of endovascular stents. Interv Cardiol Clin 5: 391-403.
17. Ng J, Bourantas CV, Torii R, Ang HY, Tenekecioqlu E, et al. (2017) Local hemodynamic forces after stenting: implications on restenosis and thrombosis. Arterioscler Thromb Vasc Biol 37: 2231-2242.
18. Stankevich KS, Gudima A, Filimonov VD, Kluter H, Mamontova EM, et al. (2015) Surface modification of biomaterials based on high-molecular polylactic acid and their effect on inflammatory reactions of primary human monocyte-derived macrophages: perspective for personalized therapy. Mater Sci Eng C Mater Biol Appl 51: 117-126.
19. Kzhyshkowska J, Gudima A, Riabov V, Dollinger C, Lavalle P, et al. (2015) Macrophage responses to implants: prospects for personalized medicine. J Leukoc Biol 98: 953-962.
20. Li J, Zou D, Zhang K, Luo X, Yang P, et al. (2017) Strong multi-functions based on conjugating chondroitin sulfate on amine-rich surface direct vascular cells fate for cardiovascular implanted devices. J Mater Chem B 5: 8299-8313.
21. Chen L, Li JA, Chang JW, Jin SB, Wu D, et al. (2018) Mg-Zn-Y-Nd coated with citric acid and dopamine by layer-by-layer self-assembly to improve surface biocompatibility. Sci China Technol Sci 61: 1228-1237.
22. Mills C (2012) M1 and M2 macrophages: oracles of health and disease. Crit Rev Immunol 32: 463-488.
23. Peled M, Fisher EA (2014) Dynamic aspects of macrophage polarization during atherosclerosis progression and regression. Front Immunol 5: 579.
24. Gombozhapova A, Rogovskaya Y, Shurupov V, Rebenkova M, Kzhyshkowska J, et al. (2017) Macrophage activation and polarization in post-infarction cardiac remodeling. J Biomed Sci 24: 13.

25. Zhou D, Huang C, Lin Z, Zhan S, Kong L, et al. (2014) Macrophage polarization and function with emphasis on the evolving roles of coordinated regulation of cellular signaling pathways. Cell Signal 26: 192-197.

26. Hume DA (2015) The many alternative faces of macrophage activation. Front Immunol 6: 370.

27. Gaffney L, Warren P, Wrona EA, Fisher MB, Freytes DO (2017) Macrophages' role in tissue disease and regeneration. Results Probl Cell Differ 62: 245-271.

28. Boersema GS, Grotenhuis N, Bayon Y, Lange JF, Bastiaansen-Jenniskens YM (2016) The effect of biomaterials used for tissue regeneration purposes on polarization of macrophages. Biores Open Access 5: 6-14.

29. Gallop JL, Walrant A, Cantley LC, Kirschner MW (2013) Phosphoinositides and membrane curvature switch the mode of actin polymerization via selective recruitment of toca-1 and Snx9. Proc Natl Acad Sci USA 110: 7193-7198.

30. Jarsch IK, Daste F, Gallop JL (2016) Membrane curvature in cell biology: An integration of molecular mechanisms. J Cell Biol 214: 3753-3787.

31. Bridges AA, Jentzsch MS, Oakes PW (2016) Micron-scale plasma membrane curvature is recognized by the septin cytoskeleton. J Cell Biol 213: 23-32.

32. Rosholm KR, Leijnse N, Mantsiou A, Tkach V, Pedersen SL, et al. (2017) Membrane curvature regulates ligand-specific membrane sorting of GPCRs in living cells. Nat Chem Biol 13: 724-729.

33. Daste F, Walrant A, Holst MR, Gadsby JR, Mason J, et al. (2017) Control of actin polymerization via the coincidence of phosphoinositides and high membranecurvature. J Cell Biol 216: 3745-3765.

34. Galic M, Begemann I, Viplav A, Matis M (2014) Force-control at cellular membranes. Bioarchitecture 4: 164-168.

35. Emmert M, Witzel P, Heinrich D (2016) Challenges in tissue engineering – towards cell control inside artificial scaffolds. Soft Matter 12: 4287-4294.

36. Recalde HR (1984) A simple method of obtaining monocytes in suspension. J Immunol Methods 69: 71-77.

37. Litman RB, Barrnett RJ (1972) The mechanism of the fixation of tissue components by osmium tetroxide via hydrogen bonding. J Ultrastruct Res 38: 63-86.

38. Berridge MV, Tan AS (1993) Characterisation of the cellular reduction of 3-(4,5-dimethylthiazol-2yl)-2,5-diphenyltetrazolium bromide (MTT): Subcellular localization, substrate dependence, and involvement of mitochondrial electron transport in MTT reduction. Archives Biochem Biophys 303: 474-482.

39. Berridge MV, Herst PM, Tan AS (2005) Tetrazolium dyes as tools in cell biology: new insights into their cellular reduction. Biotechnol Annu Rev 11: 127-152.

40. Freemerman AJ, Johnson AR, Sacks GN, Milner JJ, Kirk EL, et al. (2014) Metabolic reprogramming of macrophages. J Biol Chem 289: 7884-7896.

41. Tu TH, Kim CS, Nam-Goong IS, Nam CW, Kim YI, et al. (2015) 4-1BBL signaling promotes cell proliferation through reprogramming of glucose metabolism in monocytes/macrophages. FEBS J 282: 1468-1480.

42. Wang J, Duan Z, Nugent Z, Zou JX, Borowsky AD, et al. (2016) Reprogramming metabolism by histone methyltransferase NSD2 drives endocrine resistance via coordinated activation of pentose phosphate pathway enzymes. Cancer Lett 378: 69-79.

43. Ziegler-Heitbrock L, Ancuta P, Crowe S, Dalod M, Grau V, et al. (2010) Nomenclature of monocytes and dendritic cells in blood. Blood 116: 74-80.

44. Maharaj S, Lu K, Radom-Aizik S, Zaldivar F, Haddad F, et al. (2018) Inter- and intra-subject variability of nitric oxide levels in leukocyte subpopulations. Nitric Oxide 72: 41-45.

45. Guła Z, Stec M, Rutkowska-Zapała M, Lenart M, Korkosz M, et al. (2017) Number of circulating non-classical (CD14+CD16++) monocytes negatively correlates with DAS28 and swollen joints count in peripheral spondyloarthritis patients. Pol Arch Intern Med 127: 846-853.

46. Urbanski K, Ludew D, Filip G, Sagan A, Szczepaniak P, et al. (2017) CD14+CD16++ "nonclassical" monocytes are associated with endothelial dysfunction in patients with coronary artery disease. Thromb Haemost 117: 971-980.

47. Engel DR, Maurer J, Tittel A, Weisheit C, Cavlar T, et al. (2008) CCR2 mediates homeostatic and inflammatory release of Gr1 high monocytes from the bone marrow, but is dispensable for bladder infiltration in bacterial urinary tract infection. J Immunol 181: 5579-5586.

48. Ulrich C, Trojanowicz B, Fiedler R, Kohler F, Wolf AF, et al. (2017) Differential expression of lipoprotein-associated phospholipase A2 in monocyte subsets: impact of uremia and atherosclerosis. Nephron 135: 231-241.

49. Makinde HM, Cuda CM, Just TB, Perlman HR, Schwulst SJ (2017) Nonclassical monocytes mediate secondary injury, neurocognitive outcome, and neutrophil infiltration after traumatic brain injury. J Immunol 199: 3583-3591.

50. Thomas G, Tacke R, Hedrick CC, Hanna RN (2015) Nonclassical patrolling monocyte function in the vasculature. Arterioscler Thromb Vasc Biol 35: 1306-1316.

51. Garcia-Bonilla L, Faraco G, Moore J, Murphy M, Racchumi G, et al. (2016) Spatio-temporal profile, phenotypic diversity, and fate of recruited monocytes into the post-ischemic brain. J Neuroinflammation 13: 285.

52. França CN, Izar MC, Hortencio MN, Amaral JB, Ferreira CES, et al. (2017) Monocyte subtypes and the CCR2 chemokine receptor in cardiovascular disease. Clin Sci 131: 1215-1224.

53. Quintar A, McArdle S, Wolf D, Marki A, Ehinger E, et al. (2017) Endothelial protective monocyte patrolling in large arteries intensified by western diet and atherosclerosis. Circ Res 120: 1789-1799.

54. Trahtemberg U, Grau A, Tabib A, Atallah M, Krispin A, et al. (2016) Identification and characterization of two human monocyte-derived dendritic cell subpopulations with different functions in dying cell clearance and different patterns of cell death. PLoS One 11: e0162984.

55. Wildgruber M, Aschenbrenner T, Wendorff H, Czubba M, Glinzer A, et al. (2016) The "intermediate" CD14+ +CD16+ monocyte subset increases in severe peripheral artery disease in humans. Sci Rep 6: 39483.

56. Yang J, Zhang L, Yu C, Yang XF, Wang H (2014) Monocyte and macrophage differentiation: circulation inflammatory monocyte as biomarker for inflammatory diseases. Biomark Res 21: 1.

57. Eekhoff A, Bonakdar N, Alonso JL, Hoffmann B, Goldmann WH (2011) Glomerular podocytes: a study of mechanical properties and mechano-chemical signaling. Biochem Biophys Res Commun 406: 229-233.

58. Minner DE, Rauch P, Käs J, Naumann CA (2014) Polymer-tethered lipid multi-bilayers: a biomembrane-mimicking cell substrate to probe cellular mechano-sensing. Soft Matter 10: 1189-1198.

59. Hong J, Murugesan S, Betzig E, Hammer JA (2017) Contractile actomyosin arcs promote the activation of primary mouse T cells in a ligand-dependent manner. PLoS One 12: e0183174.

60. Rey-Giraud F, Hafner M, Ries CH (2012) In vitro generation of monocyte-derived macrophages under serum-free conditions improvestheir tumor promoting functions. PLoS One 7: e42656.

61. Heinrich F, Lehmbecker A, Raddatz BB, Kegler K, Tipold A, et al. (2017) Morphologic, phenotypic, and transcriptomic characterization of classically and alternatively activated canine blood-derived macrophages in vitro. PLoS One 12: e0183572.

62. Fais S, Burgio VL, Silvestri M, Capobianchi MR, Pacchiarotti A, et al. (1994) Multinucleated giant cells generation induced by interferon-gamma. Changes in the expression and distribution of the intercellular adhesion molecule-1 during macrophages fusion and multinucleated giant cell formation. Lab Invest 71: 737-744.

63. Helming L, Winter J, Gordon S (2009) The scavenger receptor CD36 plays a role in cytokine-induced macrophage fusion. J Cell Sci 122: 453-459.

64. Miron RJ, Bosshardt DD (2018) Multinucleated giant cells: good guys or bad guys. Tissue Eng Part B Rev 24: 53-65.

65. Collison JL, Carlin LM, Eichmann M, Geissmann F, Peakman M (2015) Heterogeneity in the locomotory behavior of human monocyte subsets over human vascular endothelium in vitro. J Immunol 195: 1162-1170.

66. Haschemi A, Kosma P, Gille L, Evans CR, Burant CF, et al. (2012) The sedoheptulose kinase carkl directs macrophage polarization through control of glucose metabolism. Cell Metab 15: 813-826.

67. Bedard K, Krause KH (2007) The NOX family of ROS-generating NADPH oxidases: physiology and pathophysiology. Physiol Rev 87: 245-313.